

# A stable vacuum from vector dark matter

*Bohdan GRZADKOWSKI*  
*University of Warsaw*

- The Vector Dark Matter (VDM) model
  - Vacuum stability
  - Landau poles
  - Experimental constraints
  - Direct detection of dark matter
  - Summary
- ◇ Mateusz Duch, B.G., Moritz McGarrie, “A stable Higgs portal with vector dark matter”, e-Print: arXiv:1506.08805

## The Vector Dark Matter (VDM) model

- T. Hambye, “Hidden vector dark matter”, JHEP 0901 (2009) 028,
- O. Lebedev, H. M. Lee, and Y. Mambrini, “Vector Higgs-portal dark matter and the invisible Higgs”, Phys.Lett. B707 (2012) 570,
- Y. Farzan and A. R. Akbarieh, “VDM: A model for Vector Dark Matter”, JCAP 1210 (2012) 026,
- S. Baek, Pyungwon Ko, W.-I. Park, and E. Senaha, “Higgs Portal Vector Dark Matter : Revisited”, JHEP 1305 (2013) 036,
- Ch. Gross, O. Lebedev, Y. Mambrini, “Non-Abelian gauge fields as dark matter”, arXiv:1505.07480,
- ...

The model:

- extra  $U(1)_X$  gauge symmetry ( $A_X^\mu$ ),
- a complex scalar field  $S$ , whose vev generates a mass for the  $U(1)$ 's vector field,  $S = (0, \mathbf{1}, \mathbf{1}, 1)$  under  $U(1)_Y \times SU(2)_L \times SU(3)_c \times U(1)_X$ .
- SM fields neutral under  $U(1)_X$ ,
- in order to ensure stability of the new vector boson, a  $\mathbb{Z}_2$  symmetry is assumed to forbid  $U(1)$ -kinetic mixing between  $U(1)_X$  and  $U(1)_Y$ . The extra gauge boson  $A_X^\mu$  and the scalar  $S$  field transform under  $\mathbb{Z}_2$  as follows

$$A_X^\mu \rightarrow -A_X^\mu, \quad S \rightarrow S^*, \quad \text{where } S = \phi e^{i\sigma}, \quad \text{so } \phi \rightarrow \phi, \quad \sigma \rightarrow -\sigma.$$

The scalar potential

$$V = -\mu_H^2 |H|^2 + \lambda_H |H|^4 - \mu_S^2 |S|^2 + \lambda_S |S|^4 + \kappa |S|^2 |H|^2.$$

The vector bosons masses:

$$M_W = \frac{1}{2} g v, \quad M_Z = \frac{1}{2} \sqrt{g^2 + g'^2} v \quad \text{and} \quad M_{Z'} = g_x v_x,$$

where

$$\langle H \rangle = \begin{pmatrix} 0 \\ \frac{v}{\sqrt{2}} \end{pmatrix} \quad \text{and} \quad \langle S \rangle = \frac{v_x}{\sqrt{2}}$$

Positivity of the potential implies

$$\lambda_H > 0, \quad \lambda_S > 0, \quad \kappa > -2\sqrt{\lambda_H \lambda_S}.$$

The minimization conditions for scalar fields

$$(2\lambda_H v^2 + \kappa v_x^2 - 2\mu_H^2)v = 0 \quad \text{and} \quad (\kappa v^2 + 2\lambda_S v_x^2 - 2\mu_S^2)v_x = 0$$

For  $\kappa^2 < 4\lambda_H\lambda_S$  the global minima are

$$v^2 = \frac{4\lambda_S\mu_H^2 - 2\kappa\mu_S^2}{4\lambda_H\lambda_S - \kappa^2} \quad \text{and} \quad v_x^2 = \frac{4\lambda_H\mu_S^2 - 2\kappa\mu_H^2}{4\lambda_H\lambda_S - \kappa^2}$$

Both scalar fields can be expanded around corresponding vev's as follows

$$S = \frac{1}{\sqrt{2}}(v_x + \phi_S + i\sigma_S), \quad H^0 = \frac{1}{\sqrt{2}}(v + \phi_H + i\sigma_H) \quad \text{where} \quad H = \begin{pmatrix} H^+ \\ H^0 \end{pmatrix}.$$

The mass squared matrix  $\mathcal{M}^2$  for the fluctuations  $(\phi_H, \phi_S)$  and their eigenvalues read

$$\mathcal{M}^2 = \begin{pmatrix} 2\lambda_H v^2 & \kappa v v_x \\ \kappa v v_x & 2\lambda_S v_x^2 \end{pmatrix}$$

$$M_{\pm}^2 = \lambda_H v^2 + \lambda_S v_x^2 \pm \sqrt{\lambda_S^2 v_x^4 - 2\lambda_H\lambda_S v^2 v_x^2 + \lambda_H^2 v^4 + \kappa^2 v^2 v_x^4}$$

$$\mathcal{M}_{\text{diag}}^2 = \begin{pmatrix} M_{h_1}^2 & 0 \\ 0 & M_{h_2}^2 \end{pmatrix}, \quad R = \begin{pmatrix} \cos \alpha & -\sin \alpha \\ \sin \alpha & \cos \alpha \end{pmatrix}, \quad \begin{pmatrix} h_1 \\ h_2 \end{pmatrix} = R^{-1} \begin{pmatrix} \phi_H \\ \phi_S \end{pmatrix},$$

where  $M_{h_1} = 125.7$  GeV is the mass of the observed Higgs particle. Then we obtain

$$\sin 2\alpha = \frac{\text{sign}(\lambda_{SM} - \lambda_H) 2\mathcal{M}_{12}^2}{\sqrt{(\mathcal{M}_{11}^2 - \mathcal{M}_{22}^2)^2 + 4(\mathcal{M}_{12}^2)^2}}, \quad \cos 2\alpha = \frac{\text{sign}(\lambda_{SM} - \lambda_H)(\mathcal{M}_{11}^2 - \mathcal{M}_{22}^2)}{\sqrt{(\mathcal{M}_{11}^2 - \mathcal{M}_{22}^2)^2 + 4(\mathcal{M}_{12}^2)^2}}.$$

Note that since vev of  $H$  is fixed at 246.22 GeV, with  $\kappa = 0$  (no mass mixing) and  $\lambda_H \neq \lambda_{SM}$  it is only  $\phi_S$  which can have the observed Higgs mass of 125.7 GeV. Even though the mass matrix is diagonal in this case, however in order to satisfy our convention that  $M_{h_1} = 125.7$  GeV a rotation by  $\alpha = \pm\pi/2$  is required in such a case.

There are 5 real parameters in the potential:  $\mu_H, \mu_S, \lambda_H, \lambda_S$  and  $\kappa$ . Adopting the minimization conditions  $\mu_H, \mu_S$  could be replaced by  $v$  and  $v_x$ . The SM vev is fixed at  $v = 246.22$  GeV. Using the condition  $M_{h_1} = 125.7$  GeV,  $v_x^2$  could be eliminated in terms of  $v^2, \lambda_H, \kappa, \lambda_S, \lambda_{SM} = M_{h_1}^2/(2v^2)$ :

$$v_x^2 = v^2 \frac{4\lambda_{SM}(\lambda_H - \lambda_{SM})}{4\lambda_S(\lambda_H - \lambda_{SM}) - \kappa^2}$$

Eventually there are 4 independent parameters:

$$(\lambda_H, \kappa, \lambda_S, g_x),$$

where  $g_x$  is the  $U(1)_X$  coupling constant.

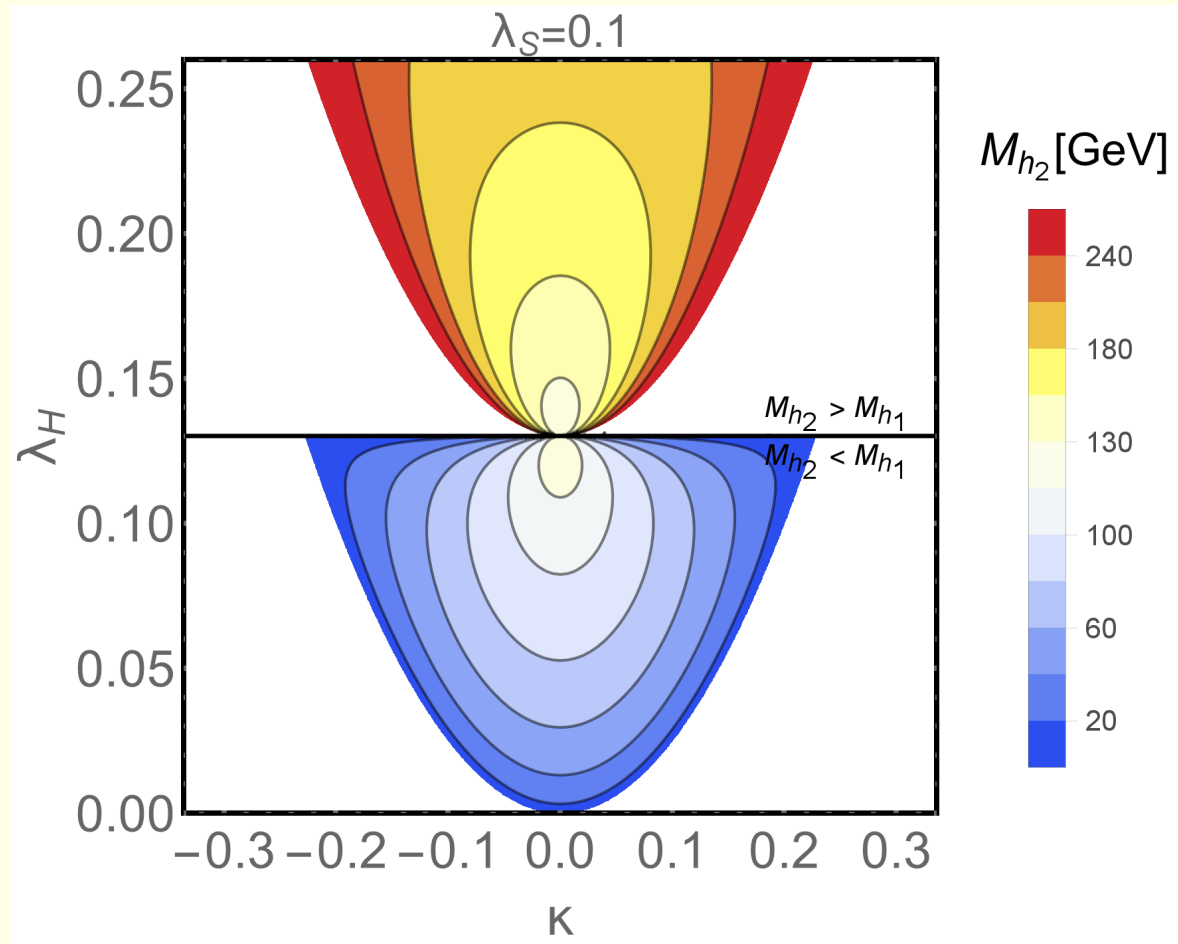


**Figure 1:** Contour plots for masses of the non-standard ( $h_2$ ) Higgs particle in the plane  $(\lambda_H, \kappa)$ . In the bottom part of the plot ( $\lambda_H < \lambda_{SM} = M_{h_1}^2 / (2v^2) = 0.13$ ) the heavier Higgs is the currently observed one, while in the upper part ( $\lambda_H > \lambda_{SM}$ ) the lighter state is the observed one. White regions in the upper and lower parts are disallowed by the positivity conditions for  $v_x^2$  and  $M_{h_2}^2$ , respectively.

- Positivity of  $v_x^2$  implies for  $\lambda_H > \lambda_{SM}$  that  $\lambda_H > \frac{\kappa^2}{4\lambda_S} + \lambda_{SM}$
- Positivity of  $M_{h_2}^2$  implies for  $\lambda_H < \lambda_{SM}$  that  $\lambda_H > \frac{\kappa^2}{4\lambda_S}$

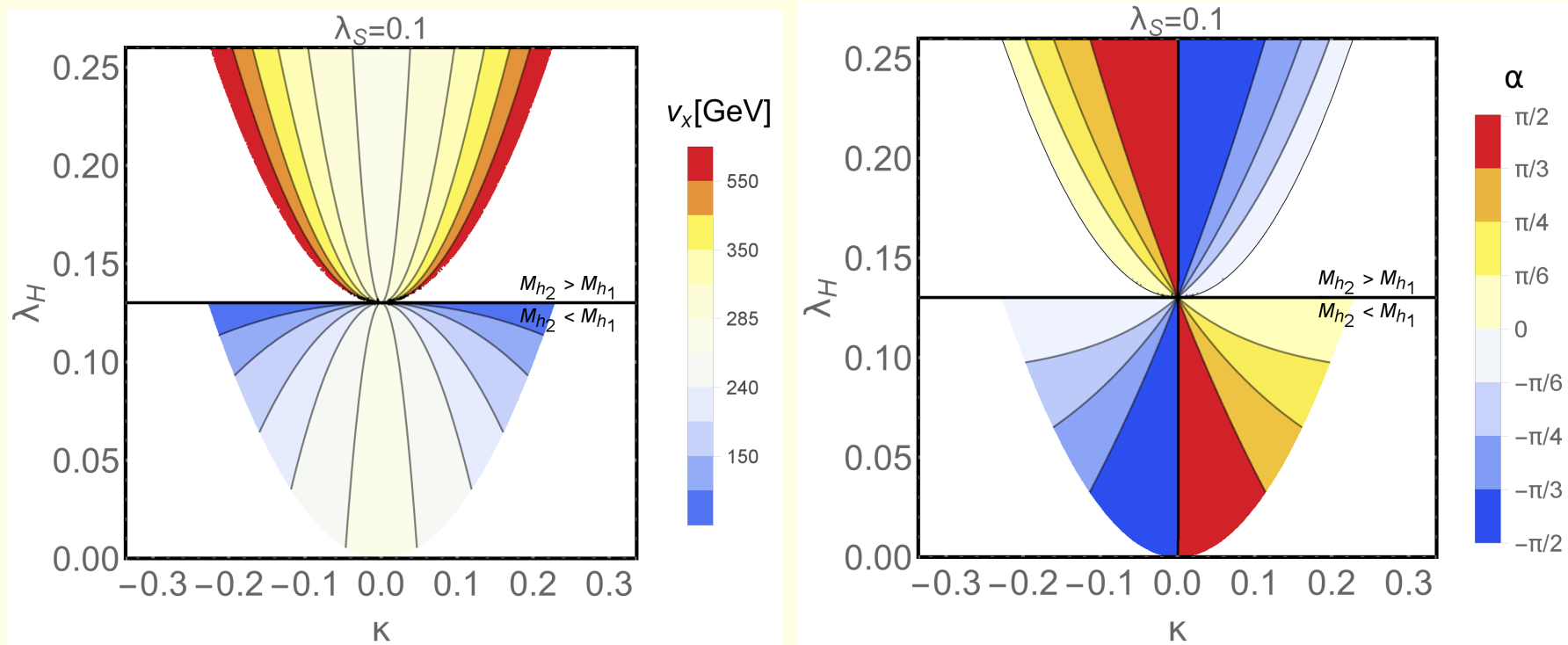


**Figure 2:** Contour plots for the vacuum expectation value of the extra scalar  $v_x \equiv \sqrt{2}\langle S \rangle$  (left panel) and of the mixing angle  $\alpha$  (right panel) in the plane  $(\lambda_H, \kappa)$ .



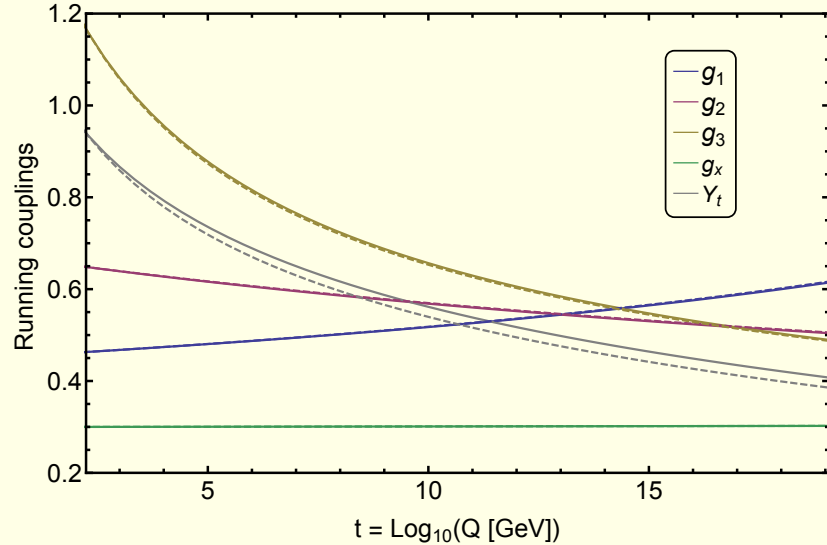
## Vacuum stability

$$V = -\mu_H^2 |H|^2 + \lambda_H |H|^4 - \mu_S^2 |S|^2 + \lambda_S |S|^4 + \kappa |S|^2 |H|^2$$

2-loop running of parameters adopted

$$\lambda_H(Q) > 0, \quad \lambda_S(Q) > 0, \quad \kappa(Q) + 2\sqrt{\lambda_H(Q)\lambda_S(Q)} > 0$$

1- (solid) and 2- (dashed) loop,  $g_x[m_t]=0.3$ ,  $\lambda_H[m_t]=0.14$ ,  $\lambda_S[m_t]=0.1$ ,  $\kappa[m_t]=-0.06$



1- (solid) and 2- (dashed) loop,  $g_x[m_t]=0.3$ ,  $\lambda_H[m_t]=0.14$ ,  $\lambda_S[m_t]=0.1$ ,  $\kappa[m_t]=-0.06$

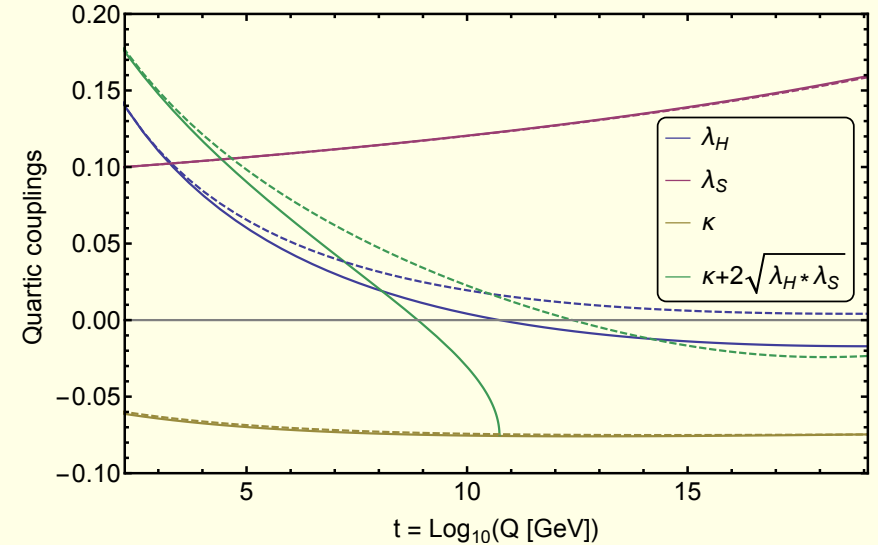


**Figure 3:** Running of various parameters at 1- and 2-loop, in solid and dashed lines respectively. For this choice of parameters  $\lambda_H(Q) > 0$  at 2-loop (right panel blue) but not at 1-loop.  $\lambda_S(Q)$  is always positive (right panel red), running of  $\kappa(Q)$  is very limited, however the third positivity condition  $\kappa(Q) + 2\sqrt{\lambda_H(Q)\lambda_S(Q)} > 0$  is violated at higher scales even at 2-loops (right panel green).

The mass of the Higgs boson is known experimentally therefore within *the SM* the initial condition for running of  $\lambda_H(Q)$  is fixed

$$\lambda_H(m_t) = M_{h_1}^2 / (2v^2) = \lambda_{SM} = 0.13$$

For VDM this is not necessarily the case:

$$M_{h_1}^2 = \lambda_H v^2 + \lambda_S v_x^2 \pm \sqrt{\lambda_S^2 v_x^4 - 2\lambda_H \lambda_S v^2 v_x^2 + \lambda_H^2 v^4 + \kappa^2 v^2 v_x^4}.$$

VDM:

- Larger initial values of  $\lambda_H$  such that  $\lambda_H(m_t) > \lambda_{SM}$  are allowed delaying the instability (by shifting up the scale at which  $\lambda_H(Q) < 0$ ).
- Even if the initial  $\lambda_H$  is smaller than its SM value,  $\lambda_H(m_t) < \lambda_{SM}$ , still there is a chance to lift the instability scale if appropriate initial value of the portal coupling  $\kappa(m_t)$  is chosen.

$$\beta_{\lambda_H}^{(1)} = \beta_{\lambda_H}^{SM(1)} + \kappa^2$$

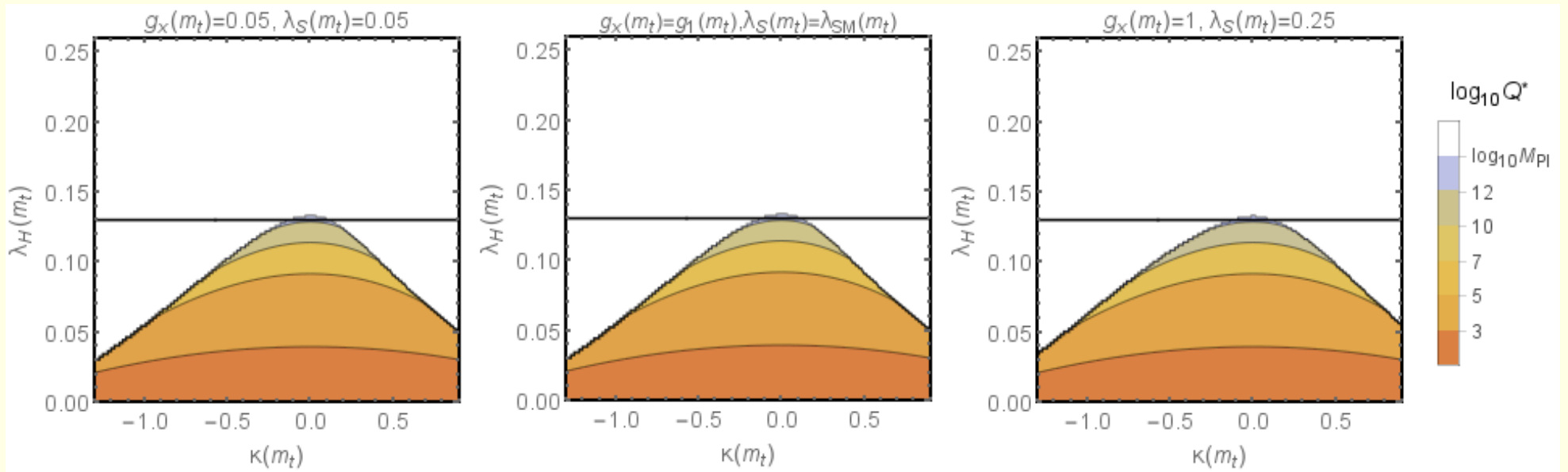


**Figure 4:** The stability frontier for the  $H$  direction: these plots identify the renormalisation scale  $t^* = \text{Log}_{10}(Q^*)$  at which  $\lambda_H(Q^*) = 0$  and the vacuum becomes unstable, as a function of  $(\lambda(m_t), \kappa(m_t))$ . The horizontal solid black line corresponds to  $\lambda_H(m_t) = \lambda_{SM} \simeq 0.13$ .

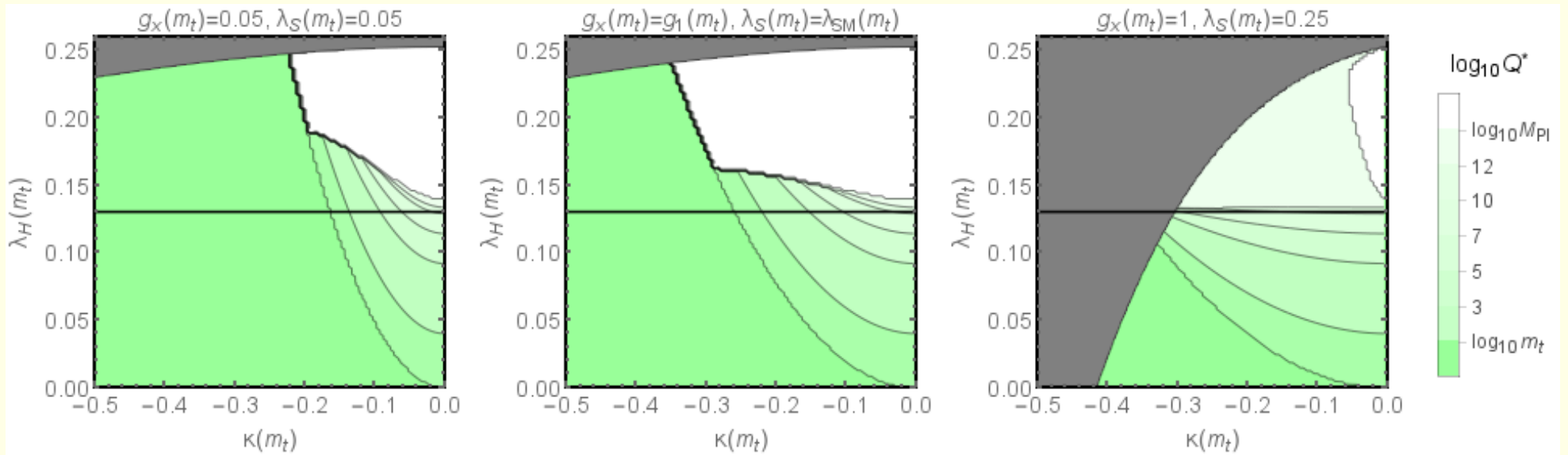


**Figure 5:** The “in between” stability frontier : these plots identify the scale  $t^* = \text{Log}_{10}(Q^*)$  at which the positivity condition  $\kappa(Q) + 2\sqrt{\lambda_H(Q)\lambda_S(Q)} > 0$  fails and the vacuum becomes unstable, as a function of  $(\lambda(m_t), \kappa(m_t))$  for fixed choices of  $(g_x(m_t), \lambda_S(m_t))$  specified above each panel. The horizontal solid black line corresponds to  $\lambda_H(m_t) = \lambda_{SM} \simeq 0.13$ . The gray area is excluded by the requirement that there is no Landau poles up to the Planck mass.

## Landau poles

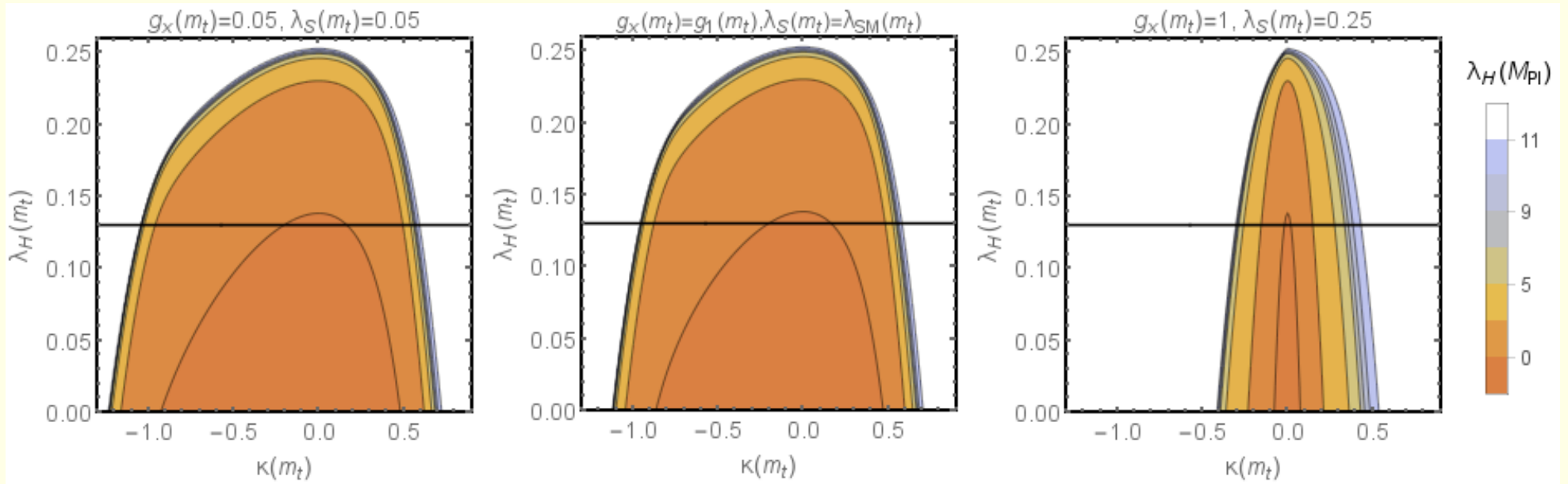


**Figure 6:** Contour plots of  $\lambda_H(M_{Pl})$  in the plane of  $(\lambda(m_t), \kappa(m_t))$  for fixed  $g_x(m_t)$  and  $\lambda_S(m_t)$  specified above each panel. The horizontal solid black line corresponds to  $\lambda_H(m_t) = \lambda_{SM} \simeq 0.13$ . The plots allow one to identify regions (white) in which the  $\lambda_H(Q)$  Landau pole is below the Planck scale.

## Experimental constraints

- no invisible  $h_1$  decays:  $h_1 \rightarrow Z'Z'$ ,  $h_1 \rightarrow h_2h_2$ ,
- LEP constraints for  $e^+e^- \rightarrow Zh_2$  satisfied,
- LHC constraints on

$$\kappa_V \equiv \frac{g_{h_1VV}}{g_{h_1VV}^{SM}} \quad \text{with} \quad 0.85 < \kappa_V < 1$$

- limits from electroweak precision data (S,T) satisfied at 95% CL

$$S = \frac{16\pi \cos^2 \theta_W}{g^2} \delta\Pi'_{ZZ}(0), \quad T = \frac{4\pi}{e^2} \left( \frac{\delta\Pi_{WW}(0)}{M_W^2} - \frac{\delta\Pi_{ZZ}(0)}{M_Z^2} \right),$$

- DM abundance ( $\Omega_{DM}h^2$ ) remains within the  $5\sigma$  limit (micrOMEGAs and explicit calculation)

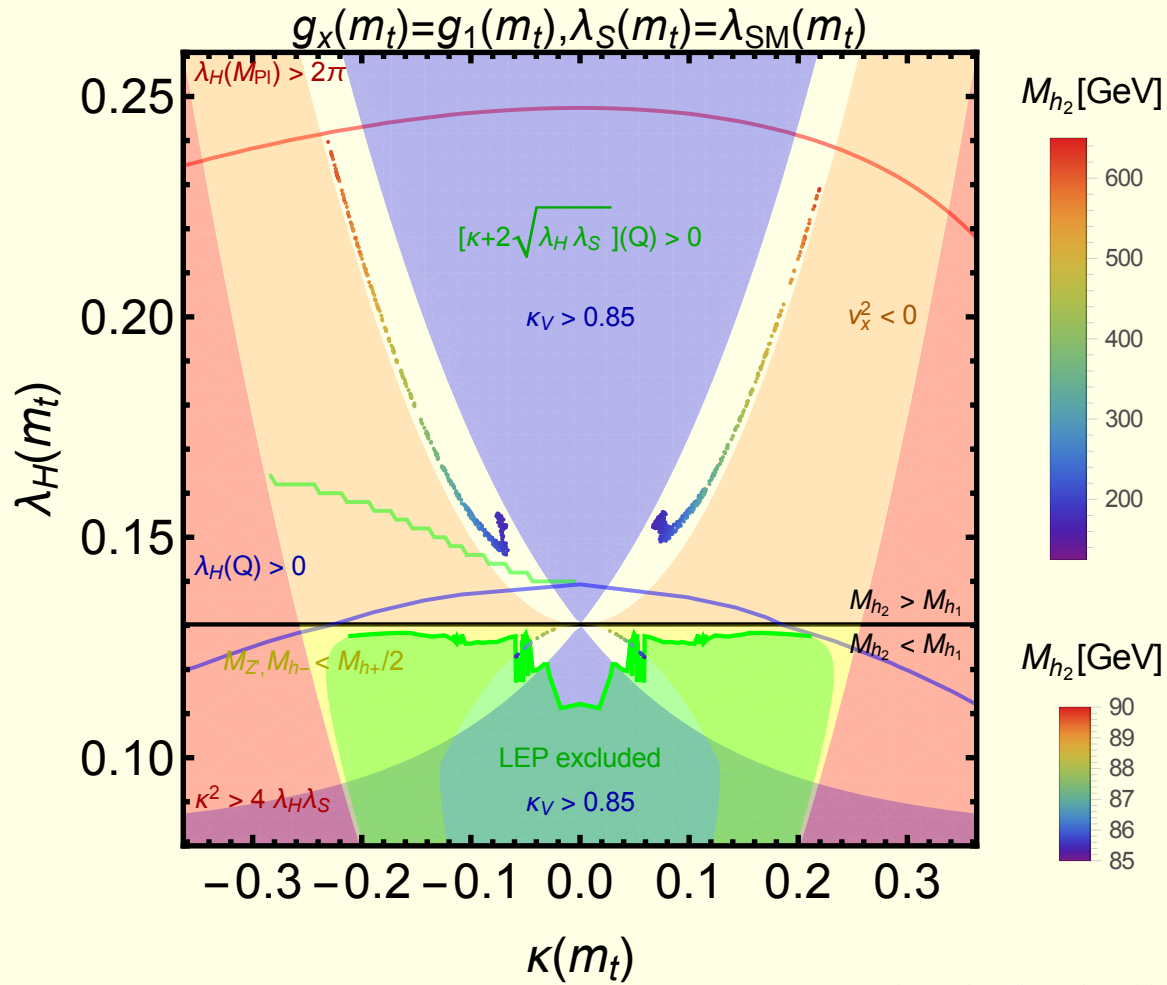


**Figure 7:** Combined plots of allowed and disallowed parameter space in the plane  $(\lambda_H(m_t), \kappa(m_t))$  for  $g_x(m_t) = g_1(m_t)$  and  $\lambda_S(m_t) = \lambda_{SM}(m_t) = 0.13$ . The thin red line denotes the frontier above which a Landau pole appears below  $\lambda_H(M_{Pl})$ . The thin blue line denotes the absolute stability frontier. Below the thin green line the positivity condition fails at some renormalisation scale (its wavy shape is a numerical artifact). The green area denotes LEP exclusions on Higgs-like scalars. In the outer red area positivity fails at the low scale, while in the orange area no physical solution of the vev  $v_x$  exists. The blue area denotes an excess of the  $h_1$  Higgs couplings to vector bosons ( $\kappa_V$ ). The remaining allowed region is in white. The green points are those for which also  $\Omega_{DM} h^2$  constraint is fulfilled.

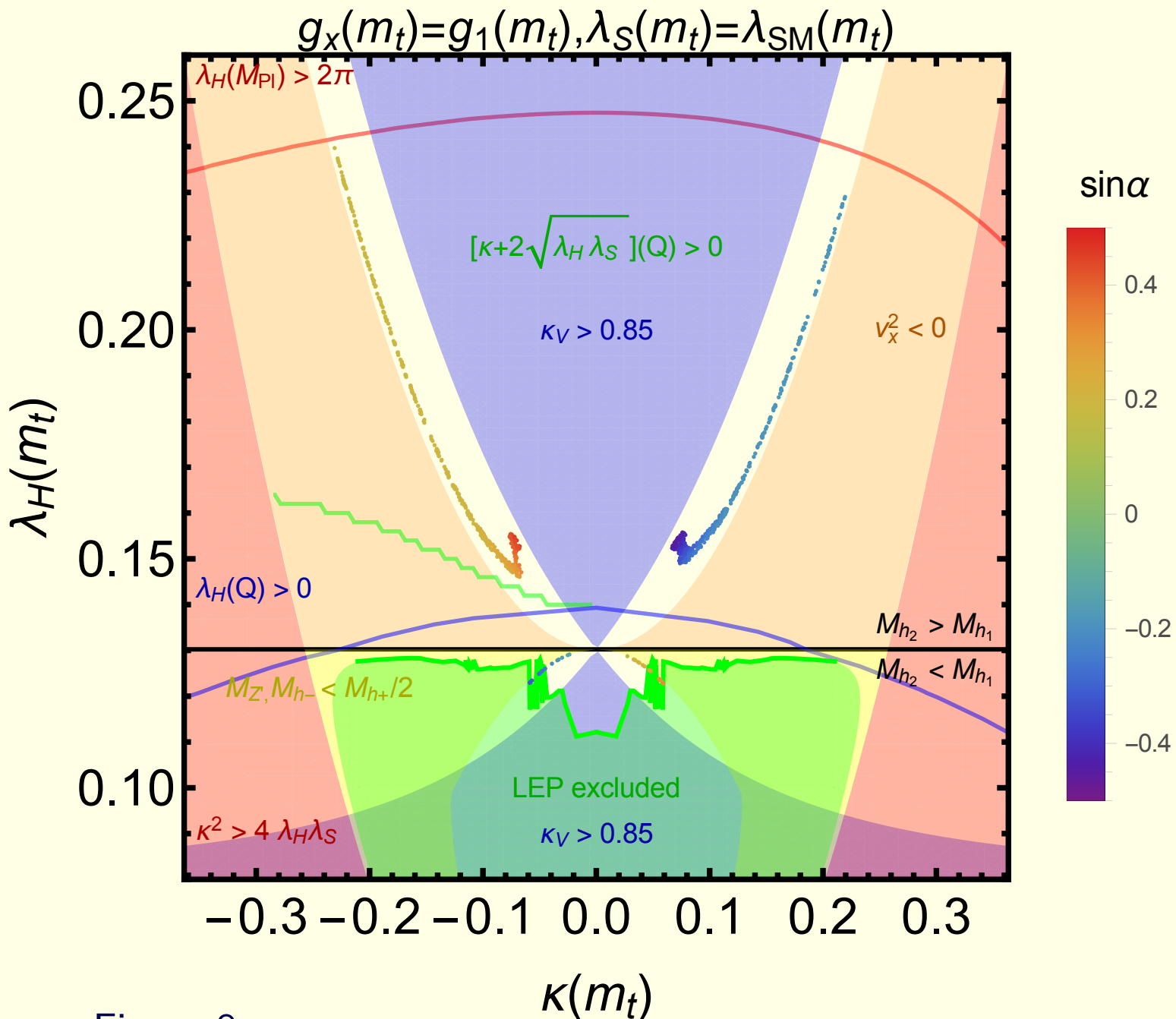
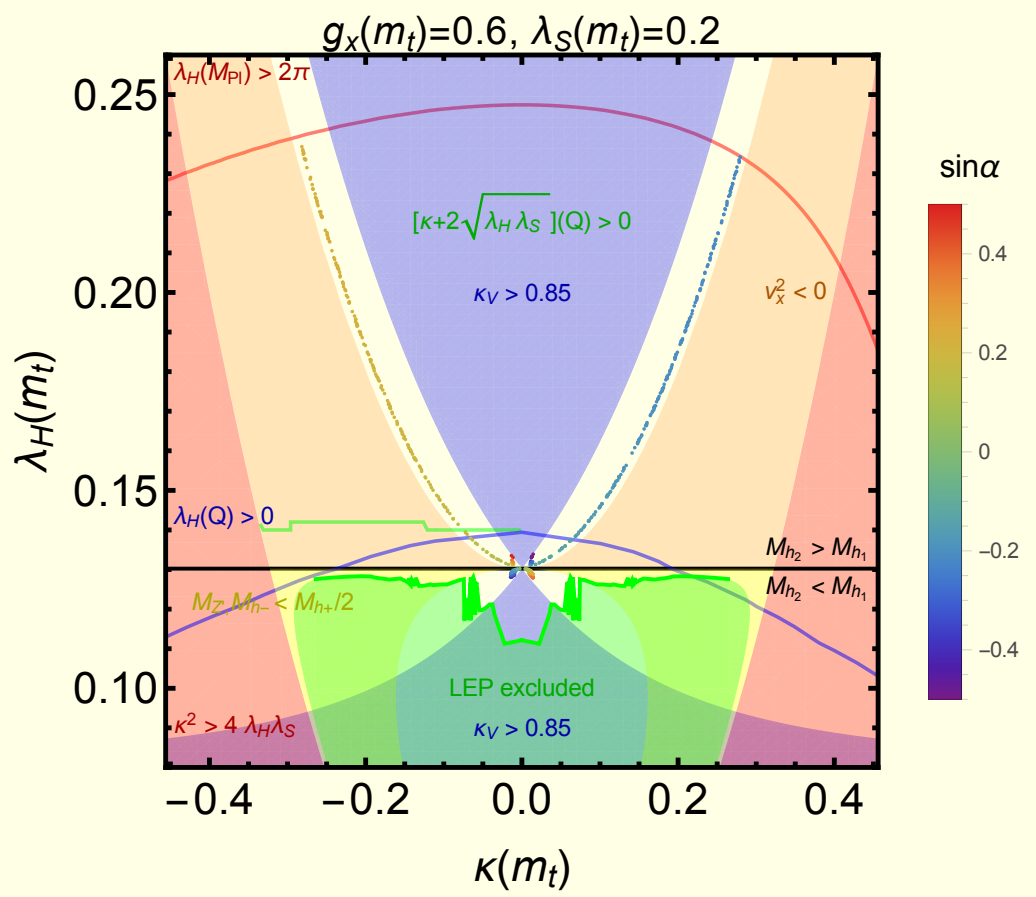
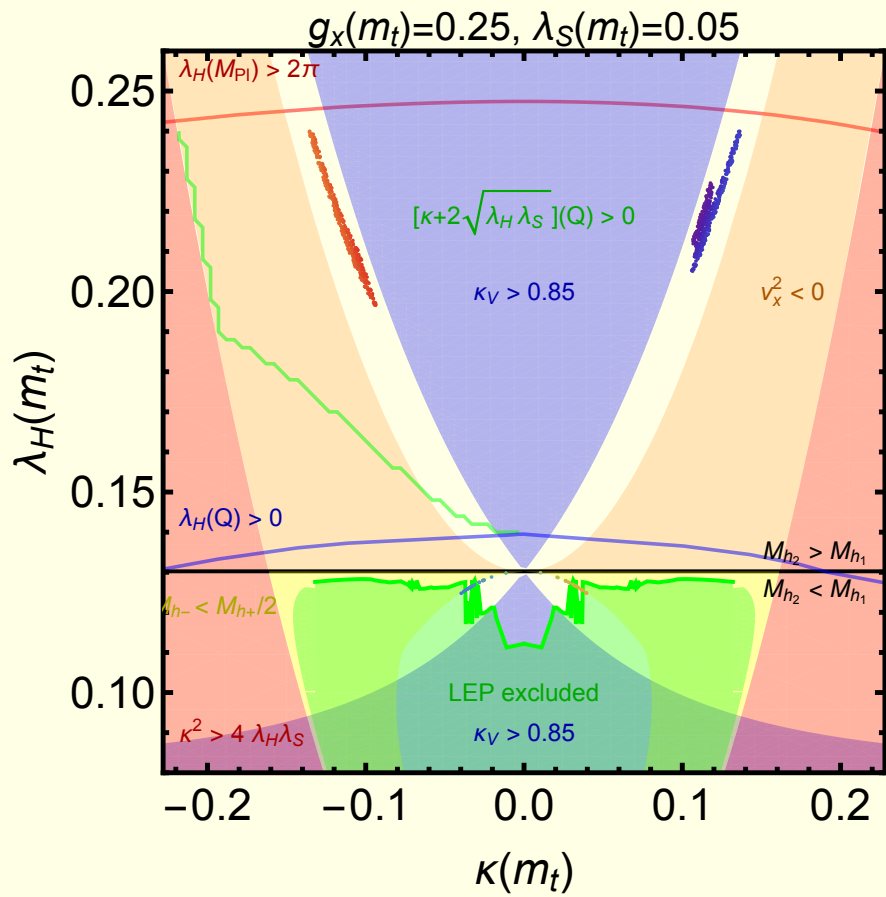


Figure 8: Same as in fig. 7 however colouring of allowed points is here with respect to  $\sin \alpha$ .

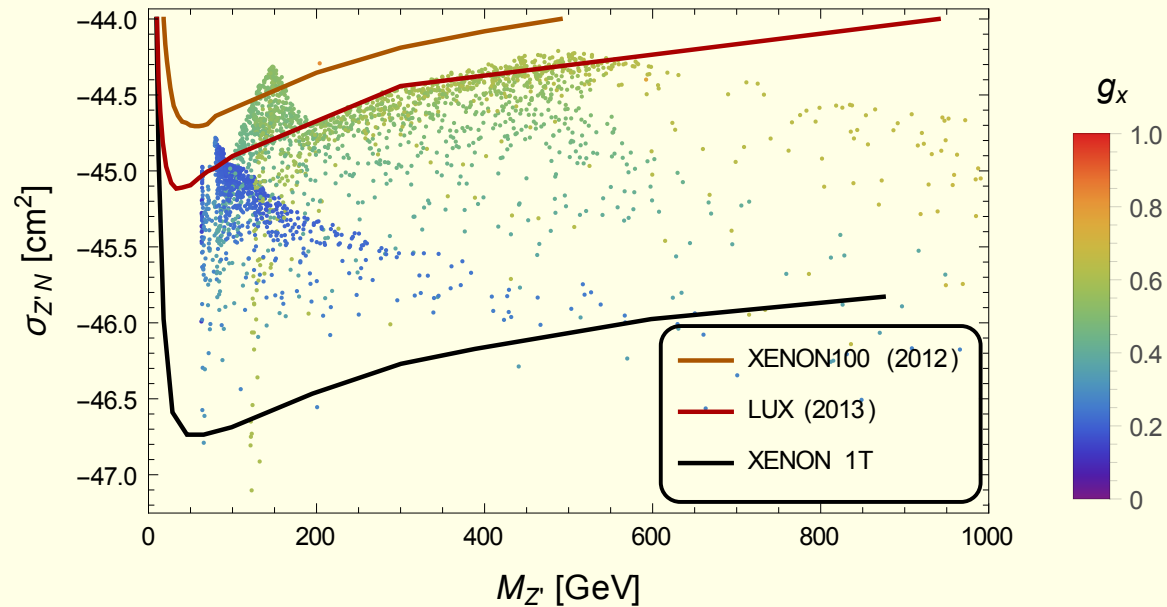




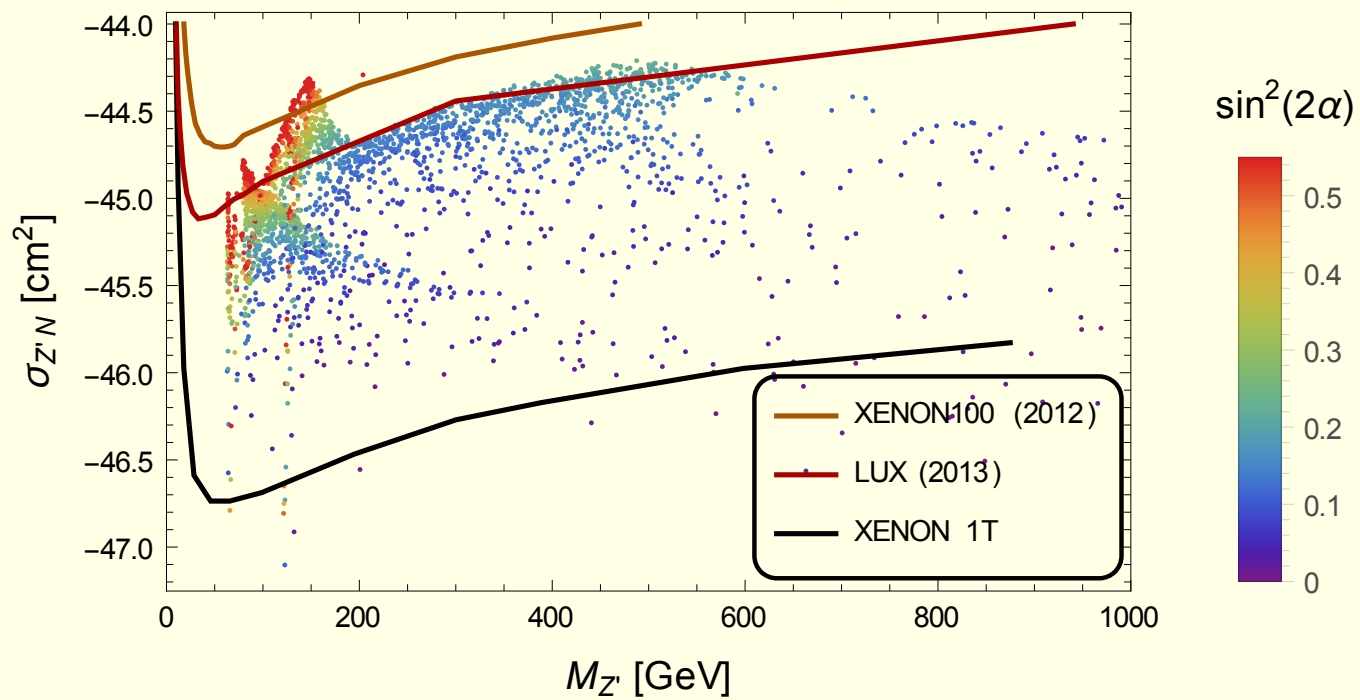
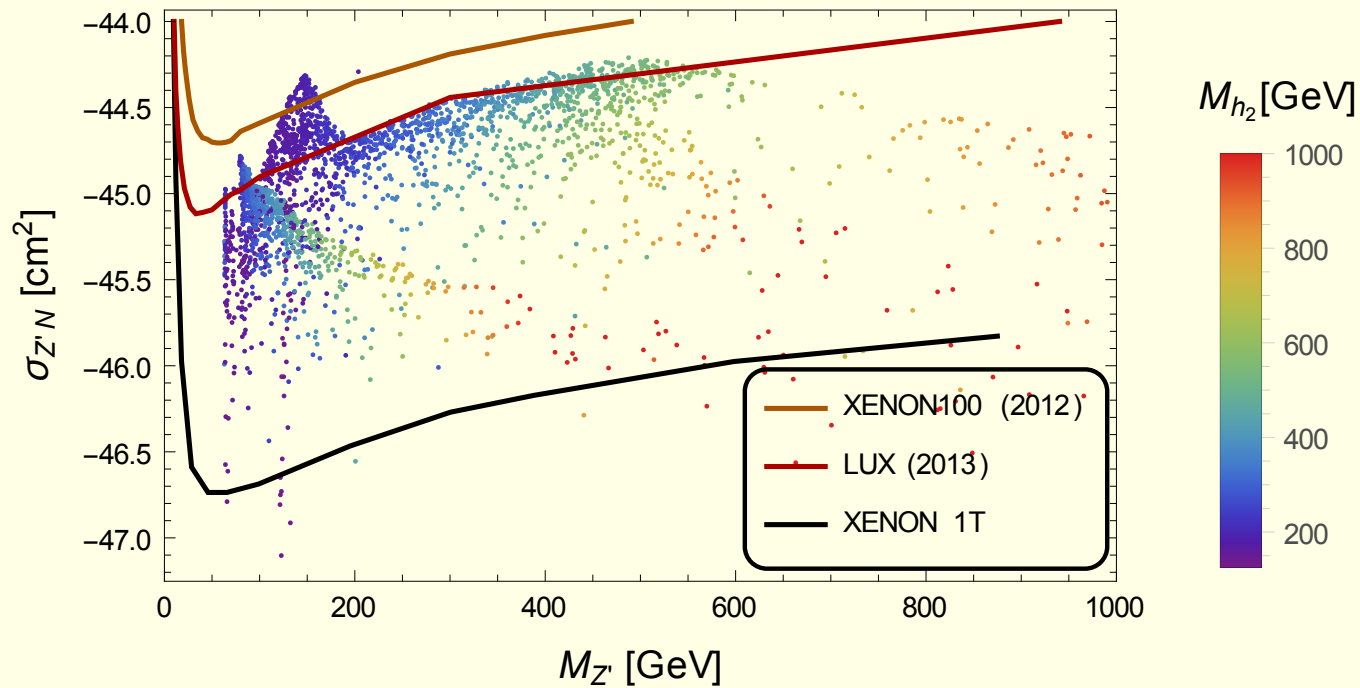
## Direct detection of dark matter

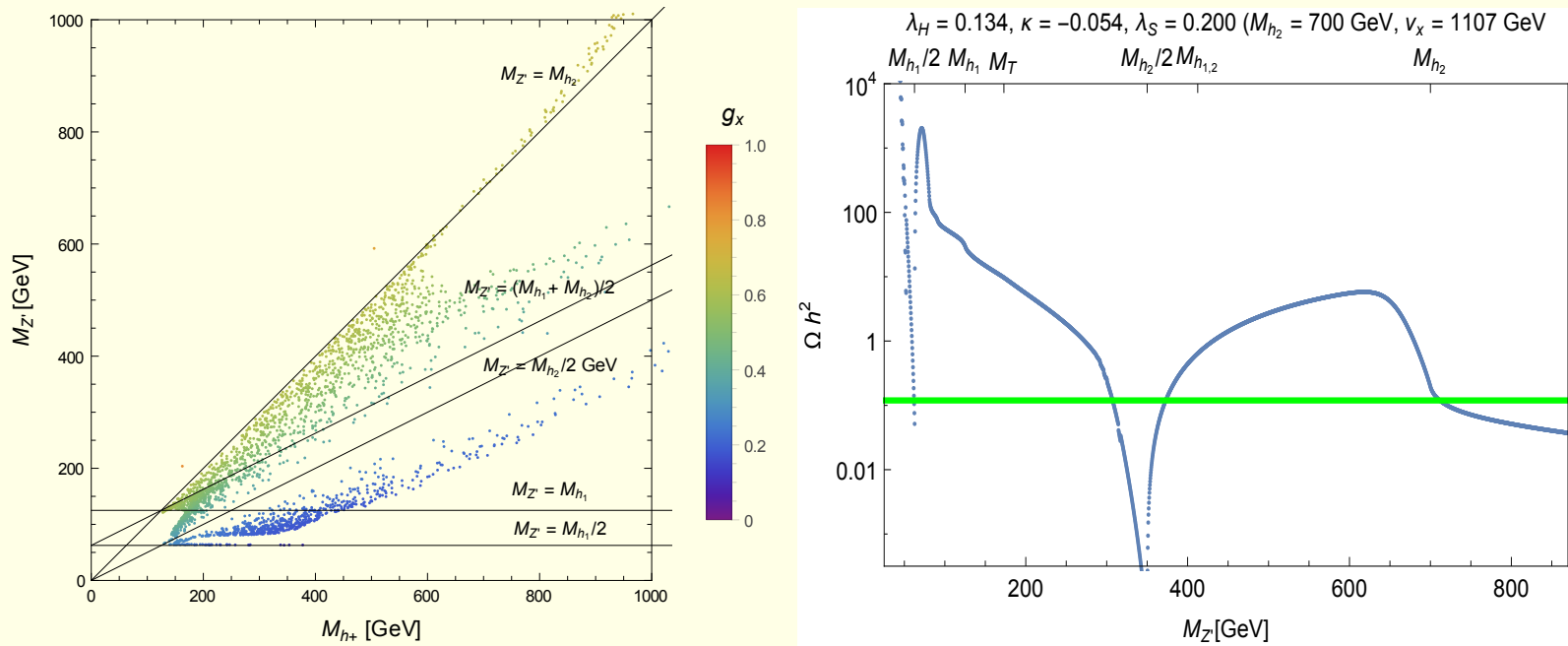
$$\sigma_{Z'N} = \frac{\mu^2}{4\pi} g_x^2 g_{hNN}^2 \sin^2 2\alpha \left( \frac{1}{M_{h_1}^2} - \frac{1}{M_{h_2}^2} \right)^2$$

- scan range:  $0.1 < g_x < 1, 0 < \lambda_H < 0.25$  and  $-0.5 < \kappa < 0.5$
- $\lambda_H > \lambda_{SM}$  (heavy dark matter):  $63 \text{ GeV} \lesssim M_{Z'} \lesssim 1000 \text{ GeV}$ .
- $\lambda_H < \lambda_{SM}$  (light dark matter):  $60 \text{ GeV} \lesssim M_{Z'} \lesssim 120 \text{ GeV}$ ,

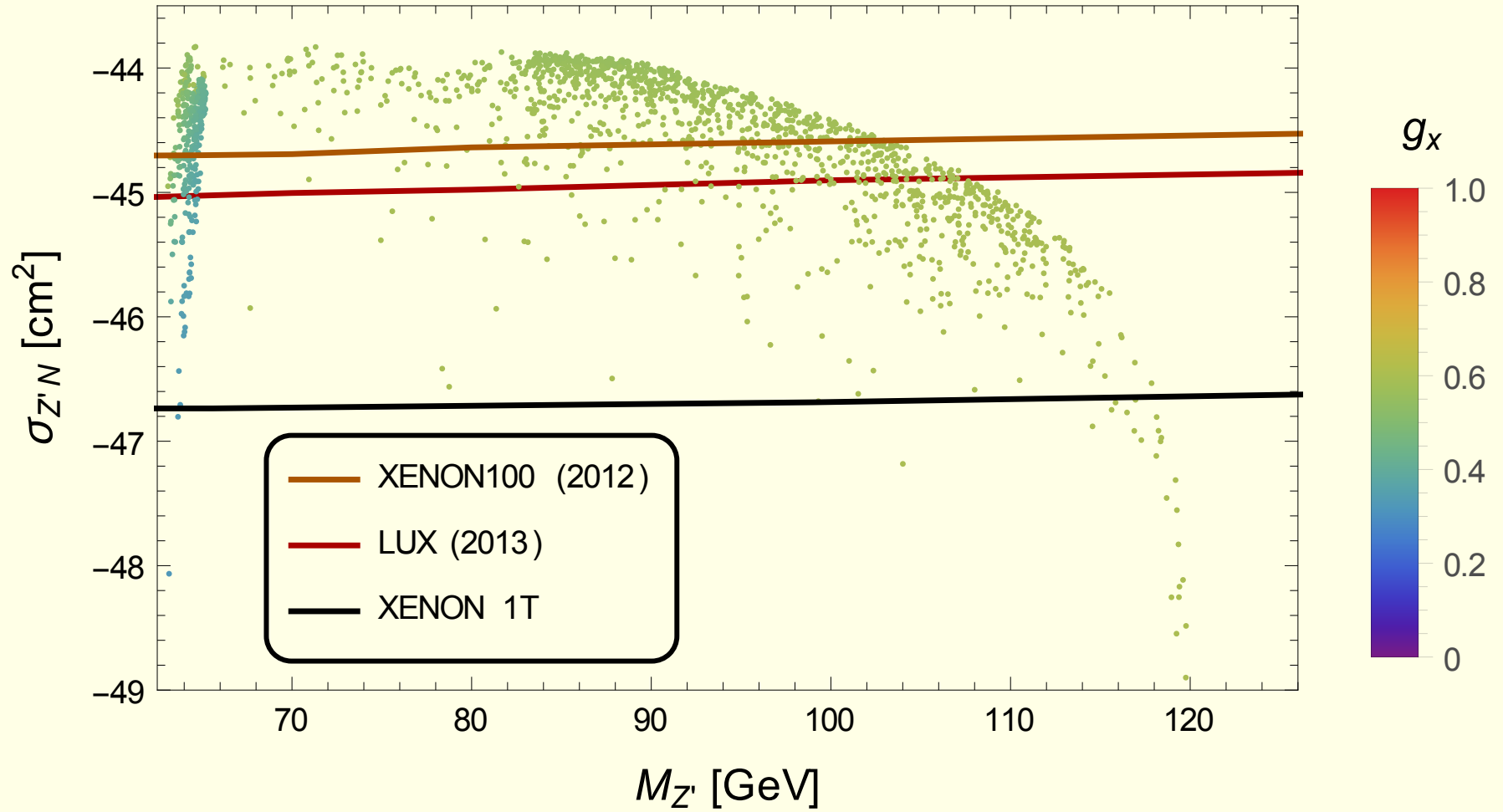


**Figure 9:** The figure shows the DM-nucleon cross section,  $\sigma_{Z'N}$ , as a function of the DM mass  $M_{Z'}$  for points which satisfy all other constraints for  $\lambda_H > \lambda_{SM}$ . The singlet quartic coupling is fixed at  $\lambda_S = 0.2$ . Colouring corresponds to the strength of the gauge coupling  $g_x$ . The solid lines are the experimental limits for  $\sigma_{Z'N}$  from XENON100, LUX (2103) and anticipated results for XENON 1T.

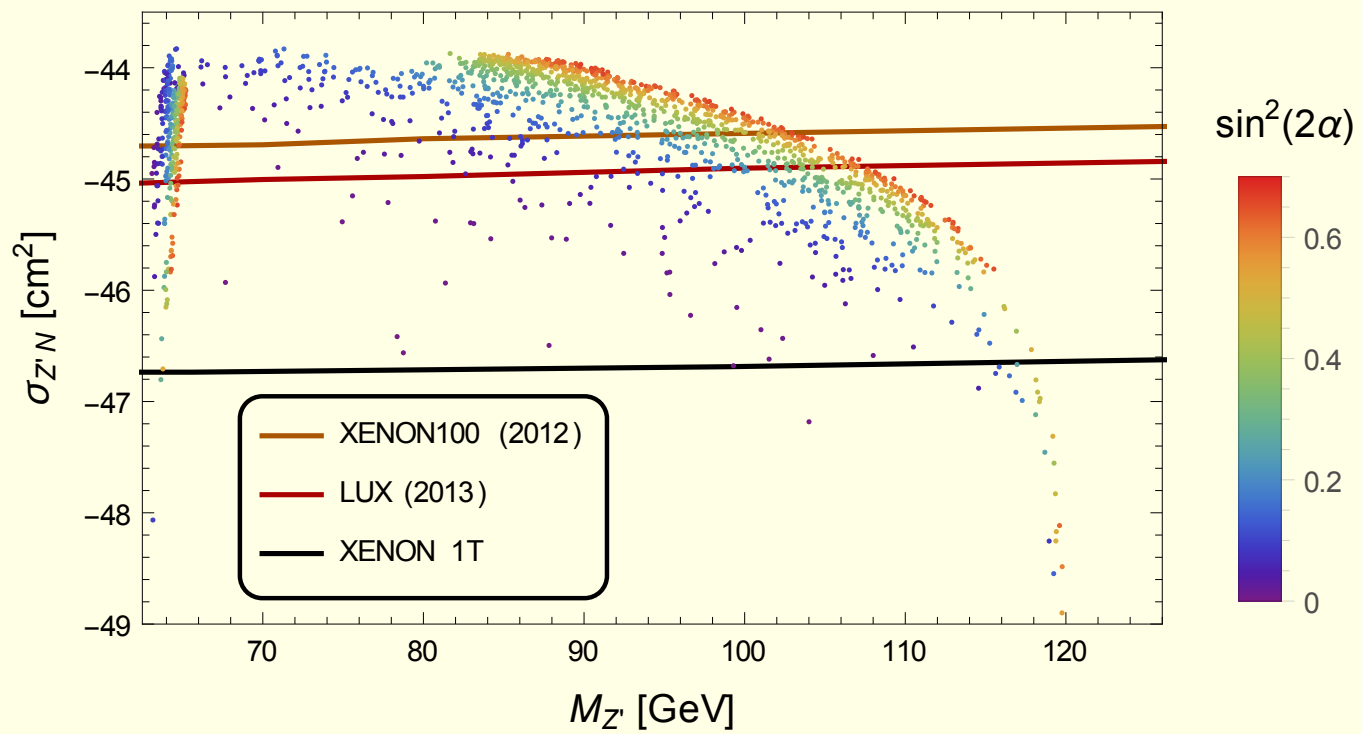
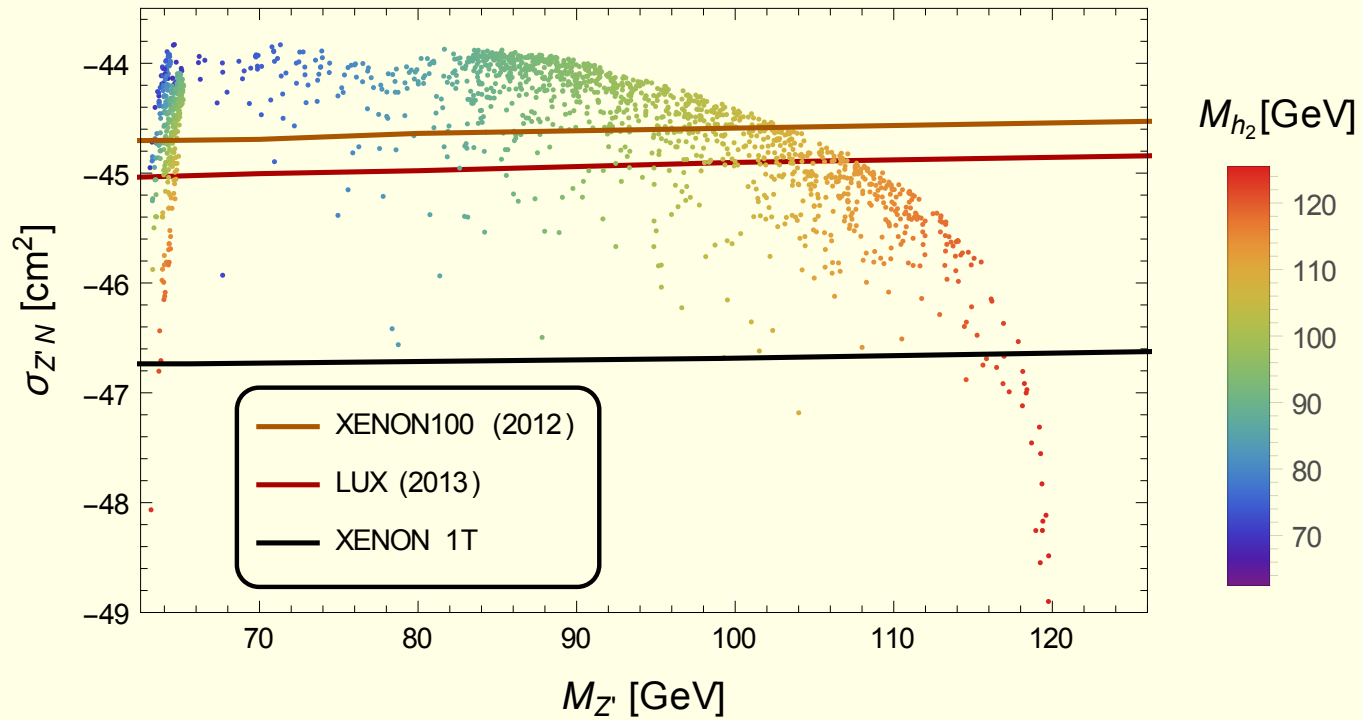




**Figure 10:** The left panel illustrates correlation between  $M_{h_2}$  and  $M_{Z'}$ , while the right one shows predictions for  $\Omega_{DM} h^2$  as a function of  $M_{Z'}$ . The colouring corresponds to the cross section  $g_x$ . Above the right box resonances and channels which open as  $M_{Z'}$  increases are shown. Coordinates in the parameter space  $(\lambda_H, \kappa, \lambda_S)$  and corresponding  $M_{h_2}$  and  $v_x$  are shown above the right panel.



**Figure 11:** The figure shows the DM-nucleon cross section,  $\sigma_{Z'N}$ , as a function of the DM mass  $M_{Z'}$  for points which satisfy all other constraints for  $\lambda_H < \lambda_{SM}$ . The singlet quartic coupling is fixed at  $\lambda_S = 0.2$ . Colouring corresponds to the strength of the gauge coupling  $g_x$ . The nearly horizontal lines are the experimental limits for  $\sigma_{Z'N}$  from XENON100, LUX (2103) and anticipated results for XENON 1T.



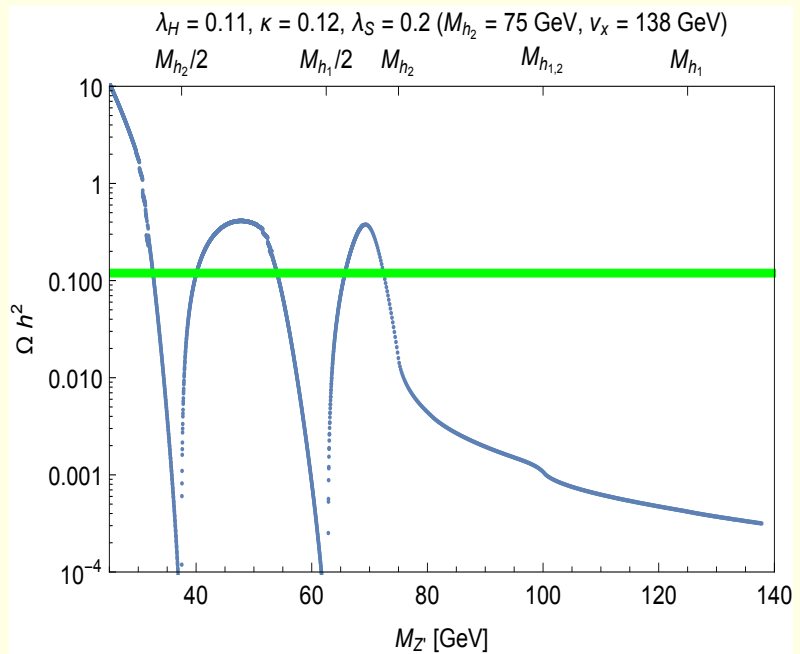
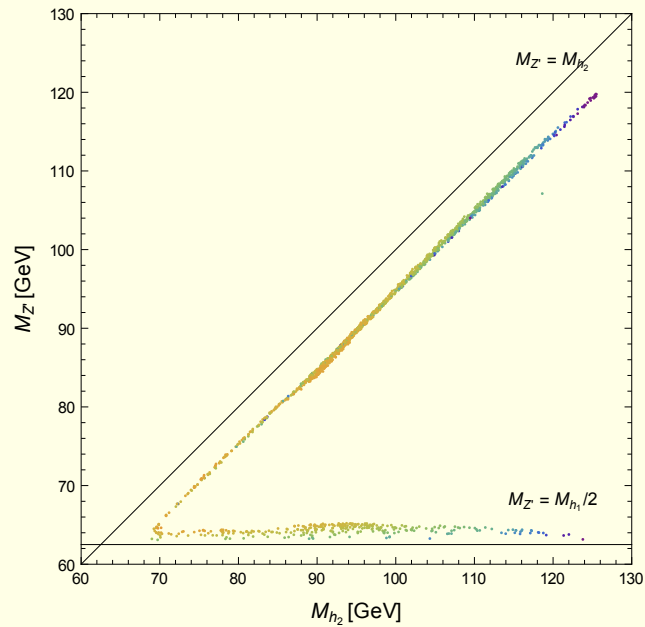


**Figure 12:** The left panel illustrates correlation between  $M_{h_2}$  and  $M_{Z'}$ , while the right one shows predictions for  $\Omega_{DM} h^2$  as a function of  $M_{Z'}$ . The colouring corresponds to the cross section  $\sigma_{Z'N}$ . Above the right box resonances and channels which open as  $M_{Z'}$  increases are shown. Coordinates in the parameter space  $(\lambda_H, \kappa, \lambda_S)$  and corresponding  $M_{h_2}$  and  $v_x$  are shown above the right panel.

## Summary

- VDM model has been presented:  $Z'$  (DM),  $h_2$  (extra Higgs)
- Vacuum stability was addressed: absolute stability
- Cosmological consequences were discussed, VDM easily consistent with  $\Omega_{DM}h^2$  and  $\sigma_{Z'N}$
- Collider phenomenology: in progress